An Experimental Method for Determining the Speed of Transverse Waves in Soap Bubbles

Nicolas Deshler and Akshay Dhar

Physics 111A Fall 2019

Contents

1 Introduction **1**
1.1 Relevant 2D Wave Theory 1
1.2 Speed of Wave Propagation in Elastic Media 3

2 Experimental Design **4**
2.1 Summary of Design Operation 4
2.2 The Circuit 5
2.3 Signal Control and Sampling 5

3 Data Acquisition and Analysis **8**
3.1 Raw Measurement Pre-Processing 9
3.2 Analysis 10

4 Discussion **14**
4.1 Experimental Results 14
4.2 Future Improvements 14

5 Supplementary Materials **15**

Abstract

We present an experimental method for determining the speed of transverse waves in soap bubble films founded on the theory of normal modes for a 2-D elastic membrane. Our method features an electronic system that acoustically drives oscillations in a circular soap bubble at fixed frequency and optically samples the surface profile using strobed illumination. By subjecting this thin membrane to a frequency scan and assessing temporal variance in the intensity of reflected light, we detect the frequencies corresponding to standing-waves. The propagation speed of transverse waves through the membrane can subsequently be calculated directly from these characteristic frequencies. Using this approach, we find the speed of transverse waves in a circular soap bubble membrane with a 7 cm diameter to be 2.21 ms^{-1}.

1 Introduction

2D wave theory reveals that the normal modes of a circular surface are physically manifest as standing waves, each with a unique characteristic frequency. We find that the propagation speed c of transverse waves in the soap bubble membrane relates to the n^{th} radially-symmetric normal mode and its characteristic frequency f_n by,

$$c = 2\pi \left(\frac{f_n}{\lambda_n} \right) \tag{1}$$

Thus the object of our experimental method is identifying standing waves and their characteristic frequencies.

The remainder of Part 1 provides theoretical background relevant to the experimental method. Part 2 describes the experimental design and circuitry. Part 3 presents and analyzes the intensity data acquired using our electronic system. Part 4 assesses the accuracy of our experimental method by comparing results to reference values.

1.1 Relevant 2D Wave Theory

Arbitrary vibrations in a 2-D membrane with a fixed circular boundary of radius $r = a$ can be decomposed into a linear combination of normal modes. Due to the geometry of our model system, it is convenient to express the normal modes as solutions to the 2-D wave equation in cylindrical coordinates. In this coordinate system, we define the origin to be coincident with the centroid of the circular boundary and the z-axis to be oriented perpendicular to the plane of the boundary. The vertical displacement of the membrane at any instant is then naturally a function of the radial and azimuthal coordinates, $u(r, \phi, t)$. For experimental convenience, we restrict our focus to situations where the membrane exhibits radial symmetry: $u(r, \phi, t) \longrightarrow u(r, t)$. Without azimuthal dependence the 2-D wave equation takes the form,

$$\left(\frac{\partial^2 u}{\partial r^2} + \frac{1}{r}\frac{\partial u}{\partial r} =\right) = \frac{1}{c^2}\left(\frac{\partial^2 u}{\partial t^2}\right) \tag{2}$$

Since the membrane is fixed at the perimeter we impose the physical boundary condition,

$$u(a,t) = 0 \tag{3}$$

Solutions to Eqn. 2 in the separable form $\Psi(r,t) = R(r)T(t)$ constitute normal modes of the system and are derived fully in [1]. For brevity, we restate the general solution for a radially-symmetric membrane below without derivation.

Radially Symmetric Solution:

$$u(r,t) = \sum_{n=1}^{\infty}(A_n cos(c\lambda_n t) + B_n sin(c\lambda_n t))J_0(\lambda_n r) \tag{4}$$

where the coefficients of the time-dependent terms are defined as,

$$A_n = \frac{2}{a^2 J_1^2(\alpha_n)}\int_0^a f(r)J_0(\lambda_n r)rdr \tag{5a}$$

$$B_n = \frac{2}{c\alpha_n a J_1^2(\alpha_n)}\int_0^a g(r)J_0(\lambda_n r)rdr \tag{5b}$$

and the initial conditions at time $t = 0$ are defined as,

$$f(r) = u(r,0) \tag{6a}$$

$$g(r) = \frac{\partial}{\partial t}u(r,0) \tag{6b}$$

Examining the series in Eqn. 4, the radial component for each term is the 0^{th}-Order Bessel Function of the first kind, $J_0(\lambda_n r)$ (Fig. 1). The constant λ_n in the argument upholds the boundary condition as it is defined to be $\frac{\alpha_n}{a}$ where α_n is the n^{th} root of J_0 and has units of inverse meters m^{-1}. This way, when $r = a$ all terms in the series go to zero.

Armed with a general description of the radially-symmetric membrane, we must point out that the Bessel functions preserve a vital orthogonality property derived in [2].

$$\int_0^a J_0(\lambda_m r)J_0(\lambda_n r)rdr = \begin{cases} \frac{1}{2}J_0'^2(\lambda_n) & m = n \\ 0 & m \neq n \end{cases} \tag{7}$$

Comparing the integral in the Eqn. 7 to the integrals in Eqn. 5, it follows that if the membrane is initially in a single normal mode (i.e. if $f(r)$ or $g(r)$ are equal to $J_0(\lambda_m r), m = 1, 2, 3...$), the coefficients A_n and B_n for the time-dependent terms will be non-zero for only these modes. The time-dependent

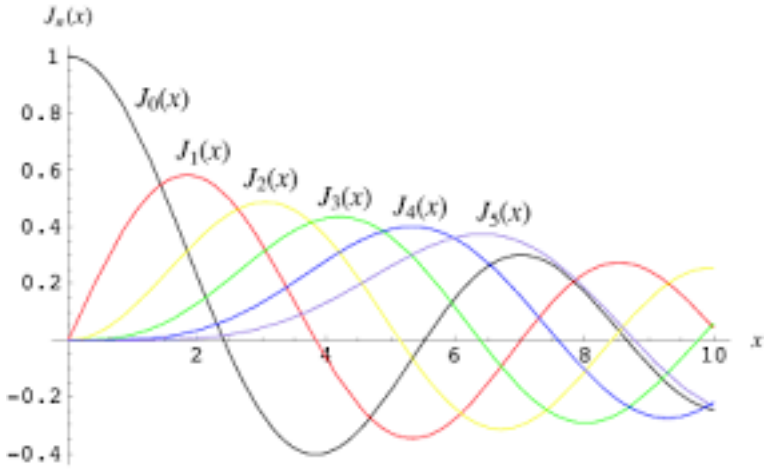

Figure 1: The Bessel Functions of the first kind. The solutions to the 2D wave equation contain only $J_0(\lambda_n r)$ which has an infinite number of roots α_n

part then just serves to periodically scale the amplitude of the surface described by the radially-dependent part. This observation is important because it indicates that the normal modes are manifest as standing waves in the membrane. Moreover, it indicates that each normal mode has a unique characteristic oscillation frequency.

Equating the argument of the sinusoidal time-dependent terms in Eqn. 4 to the standing-wave frequency, we recover Eqn. 1

$$c\lambda_n t = \omega t = 2\pi f_n t$$

$$c = 2\pi \left(\frac{f_n}{\lambda_n} \right)$$

1.2 Speed of Wave Propagation in Elastic Media

The propagation speed c of transverse waves through an elastic 2D surface can be derived from Newtons Laws assuming the displacement of the surface is very small [3]. We restate the conclusions of this derivation below.

$$c = \sqrt{\frac{\gamma}{\sigma}} \tag{8}$$

Here, γ is the surface tension in the membrane and σ is the surface density. The two quantities on the right-hand side of the equality are easily measurable and can be used to validate the wave speed found using Eqn. 1.

2 Experimental Design

2.1 Summary of Design Operation

Our experimental system employs a cymatic technique to distinguish between standing waves and transient waves. Under strobed illumination standing waves 'become' fixed surfaces; provided the strobe frequency matches the characteristic frequency. In other words, the topography of the membrane appears unchanging. In contrast, transient waves appear erratic under strobed illumination. The starkly different optical effects that these two wave regimes produce when exposed to strobed illumination can therefore be be exploited to distinguish between them. For standing waves, we can expect the distribution of reflected light intensity over all solid angles above the membrane to remain approximately constant across instances when the strobe light is on. For transient waves, we can expect the intensity distribution to vary substantially over time. Guided by these assumptions, our electronic system is designed to measure the temporal change in the intensity of reflected light coming off of the surface of soap bubble membrane.

We excite the soap bubble membrane into its normal modes by subjecting it to a sinusoidal acoustic drive generated with a speaker. Synchronously, a square-wave drive with equal frequency is sent to an LED, creating the strobe effect. A photodiode placed above the surface and tilted parallel to the angle of reflection continuously transmits intensity information to a data acquisition board (Fig. 2).

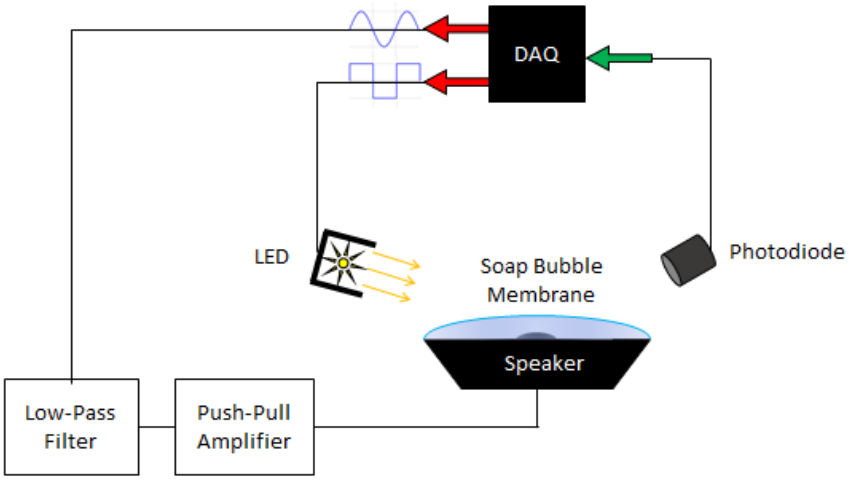

Figure 2: An illustration of the configuration for the primary components of the experimental design.

2.2 The Circuit

The circuit designed for this system (Fig. 3) serves as the interface between the DAQ and the physical phenomena at play in the membrane. The sine-wave (AO-0) and square-wave (AO-1) signals generated by the DAQ are inherently discretized. While this is a non-issue for the square-wave signal, the sine-wave signal requires low-pass filtering to smooth away any step-wise features. Thus, the signal is first corrected with a second-order RC low-pass filter designed to have a cutoff frequency equal to 482 Hz - roughly double the maximum frequency in our scan range.

The impedance of the speaker was measured to be 4Ω. As the DAQ alone cannot supply sufficient current to preserve a constant peak voltage drop across such a low-impedance component, we decouple the DAQ from the speaker via a push-pull amplifier with a 10× gain. This ensures that the speaker head displacement (the volume) is consistent for all drive frequencies. Under this configuration we found that the Vpp of the acoustic drive signal sent to the speaker remained consistent through the frequency scan range (Fig. 4).

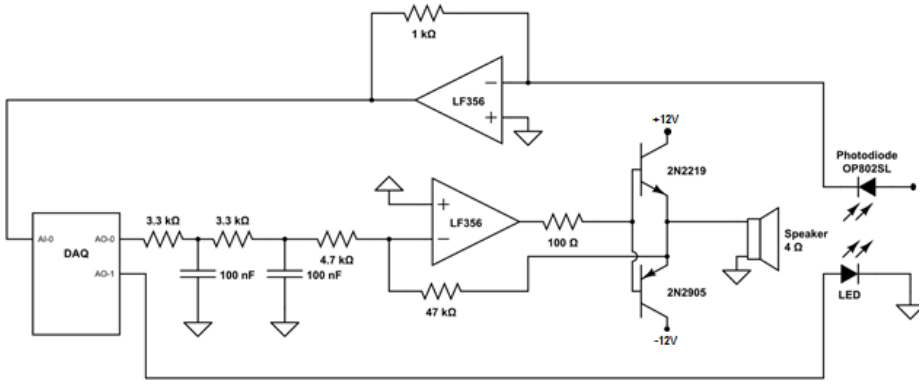

Figure 3: Circuit diagram of data acquisition system.

2.3 Signal Control and Sampling

Two LabVIEW programs (shown in Fig. 6 and Fig. 7) were written to control the signals sent from the DAQ output channels. Using these tools we subject the membrane to an acoustic frequency scan between 10 : 205 Hz incrementing in 1 Hz steps. The DAQ was configured to transmit and write signals at 10 kHz. This is well above the Nyquist rate for all frequencies traversed in the scan. For each frequency, we sampled continuously for 5 seconds, amounting to a total of 50k samples per frequency. These programs enable precise control over various signal parameters including frequency, amplitude, phase, and waveform. Importantly, the phase of the strobe is offset to optically sample standing wave at the peak of its oscillation which is $\pi/2$ rads out of phase with the drive

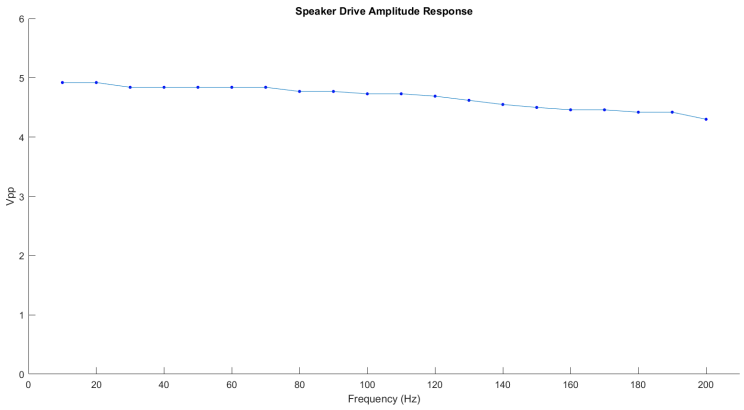

Figure 4: Amplitude response of the sinusoidal acoustic drive. Displayed voltage measurements are Vpp

frequency when in resonance (Fig. 5). This is presumably when the rate-of-change in the standing wave's transverse motion is at a minimum, lending to a more consistent light intensity distribution above the membrane. A summary of the experimental signal and sampling settings is shown in Table 1.

Table 1: **Drive Signals and Sampling Details**

Acoustic drive Vpp	4.66 V
LED drive Vpp	10 V
LED drive duty-cycle	25%
DAQ sample rate	10 kHz
Frequency scan range	$10 - 205$ Hz
Samples per frequency	50 k

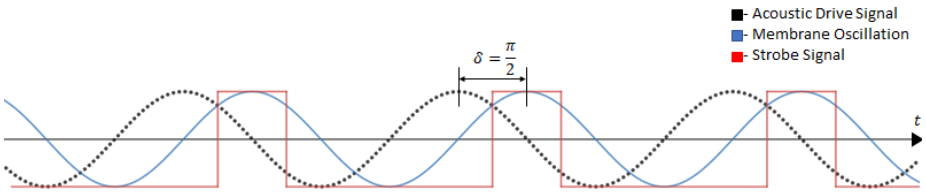

Figure 5: A graphical illustration of the phase and frequency relationships between the acoustic drive signal, the strobe signal, and a resonant standing wave. The strobe is set to optically sample the standing wave around the peak of its oscillation. Around this point the velocity of the transverse motion in the membrane is at a minimum, so the temporal variation of the reflected light distribution is similarly minimal.

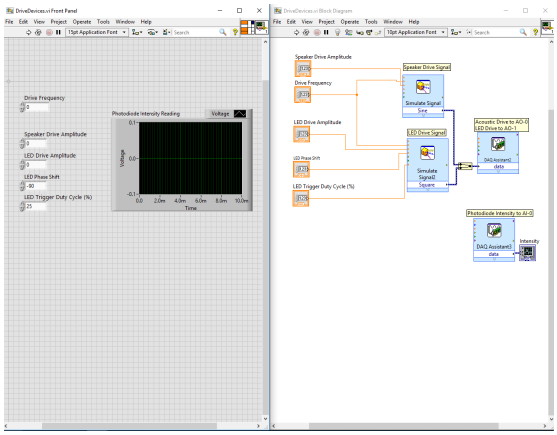

Figure 6: Front panel and back panel for our LabVIEW program DriveDevices.vi. This program controls the DAQ output signal parameters.

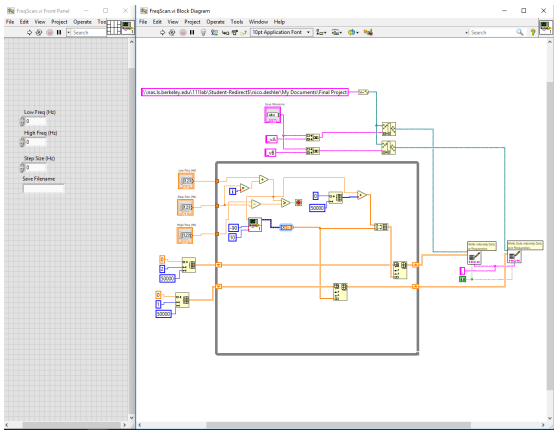

Figure 7: Front panel and back panel for our labAVIEW program FreqScan.vi. This program controls the frequency scan parameters and writes the intensity data.

3 Data Acquisition and Analysis

The decision to restrict the focus of our investigation to the radially-symmetric normal modes of the membrane stems from the realization that these modes are easy to visually observe and classify in an experimental setting compared to normal modes with azimuthal dependence. Within the frequency scan, we see the first six radially-symmetric modes appear near the drive frequencies listed in Table 2. Validating the accuracy of our mode-detection algorithm becomes tenable given our visual observations of the radially-symmetric modes. The algorithm designed to process our temporal intensity data seeks to rediscover these characteristic frequencies; hence determining the propagation speed of transverse waves through the soap bubble medium. A high-level summary of the steps involved in our data processing pipeline is provided below.

Data Processing Pipeline Summary:

1. Bin the temporal intensity measurements by drive frequency
2. Splice and concatenate the measurements to isolate signal when the strobe light is on
3. Digitally low-pass filter the signals to remove high-frequency noise above their drive frequency
4. Compute the temporal variance of the intensity for each signal
5. Search for the transverse wave speed that would minimize the sum of variances among the first 6 characteristic frequencies

3.1 Raw Measurement Pre-Processing

On their own, the raw intensity measurements collected for each drive frequency reveal little about the presence of a standing wave in the membrane due to the strobed illumination. Two processing steps are conducted to the intensity data collected for each drive frequency in preparation for the analysis. First, moments in the data acquisition timeline where the strobe light is on are spliced and concatenated (Fig. 8). Intensity measurements corresponding to the time where light is off are useless. Second, the concatenated signal is digitally low-pass filtered above the drive frequency, effectively removing noise (Fig. 9). This second step is executed because we only expect to see physically relevant phenomena varying at the timescales of the acoustic drive for standing waves. Any higher frequency content is noise in the signal that may affect the analysis.

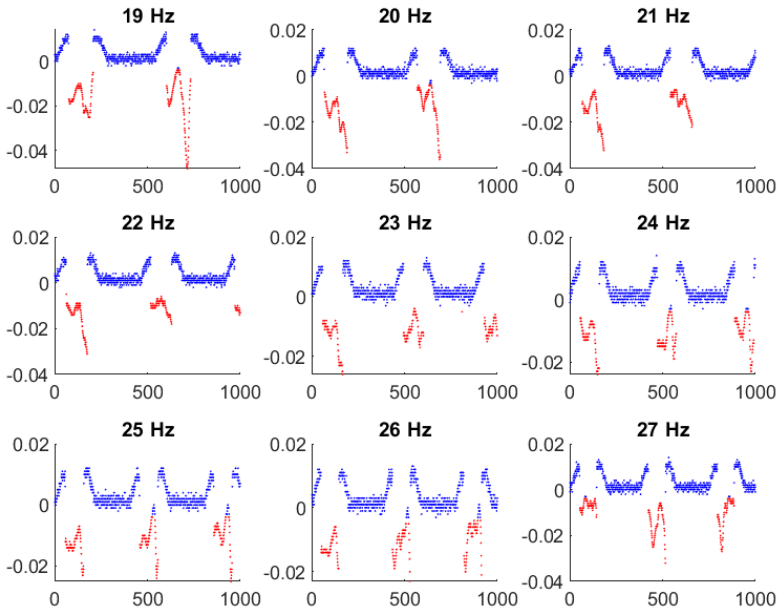

Figure 8: Spliced signals (red points) extracted from raw intensity signals (blue points) for an arbitrary subset of frequencies in the scan range. The spliced signals correspond to moments where the LED is on and illuminating the soap bubble membrane.

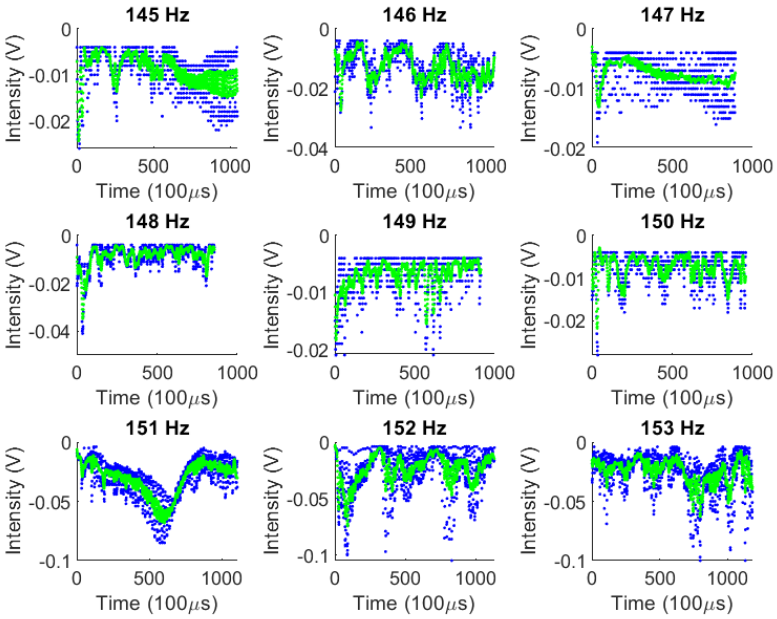

Figure 9: Comparison of the concatenated signal before (blue points) and after (green points) applying a digital low-pass filter with cutoff frequency equal to the drive frequency for noise removal. The subset of drive frequencies from the scan shown here is arbitrary.

3.2 Analysis

The temporal variance of the concatenated intensity signal serves as a quantitative measure of how constant the reflected light distribution is over time. By extension, it indicates whether or not the membrane exhibits a standing wave at a particular drive frequency. Fig. 10 shows the variance in reflected light intensity all drive frequencies in the scan. For characteristic frequencies of standing waves, we expect the variance to be small compared to transient waves. It is important to note that standing waves with azimuthal dependence also appear in the frequency scan. This poses a challenge to isolating the characteristic frequencies corresponding only to the radially-symmetric modes. To solve this, we pose a minimization problem which exploits knowledge of the relative separation between the roots of J_0.

Minimization Problem:
Let us define $I : I(c)$, a function of the transverse wave speed through the membrane, as

$$I(c) = \sum_{n=1}^{6} V[f_n(c)] \tag{9}$$

$V : V[f]$ is a vector containing our intensity variance data (Fig. 10) and f_n is the characteristic frequency of the n^{th} radially-symmetric normal mode. Reorganizing Eqn. 1 we see that the characteristic frequencies are solely dependent on the wave speed

$$f_n = \frac{\alpha_n}{2\pi a} c \tag{10}$$

since the roots α_n are known constants and the radius a is an experimental parameter. The relative separation of the first six roots of J_0 are presumed to be unique and non-redundant among the set of all roots for Bessel functions of the first kind. The relative positions of the first six characteristic frequencies are thus rigidly set via Eqn. 10. Varying c effectively scales these separations. By exploring different values for c and assessing the total intensity variance of the resulting f_n's given by Fig. 10, we can identify a scaling for which the total intensity variance is a minimum. This amounts to searching for the wave speed c for which $I(c)$ is a minimum.

$$c^* = \arg\min_c I(c) = \arg\min_c = \sum_{n=1}^{6} V\left[\left\lfloor \frac{\alpha_n}{2\pi a} c \right\rfloor\right] \tag{11}$$

$I(c)$ is not convex so instead of using optimization techniques, we computationally conduct a naive search for the minimizing value of c over the domain of wave speeds (scalings) that permit all six characteristic frequencies to exist within the frequency scan range.

$$\frac{f_{\text{scan}_{min}}}{\alpha_1} \leq \frac{c}{2\pi a} \leq \frac{f_{\text{scan}_{max}}}{\alpha_6}$$

The results of the search are shown graphically in Fig. 11. From this analysis, we conclude that the speed of propagation for transverse waves through the soap bubble membrane is 2.21 ms^{-1}. For comparison, we plot the sets of observed and computed characteristic frequencies in Fig. 12 along with their respective temporal intensity variances.

Characteristic Frequencies	f_1 Hz	f_2 Hz	f_3 Hz	f_4 Hz	f_5 Hz	f_6 Hz	**c ms^{-1}**
Observed	27	62	97	129	167	202	**2.45**
Computed	24	55	87	119	150	182	**2.21**

Table 2: Comparison of characteristic frequencies for first six radially-symmetric normal modes found using visual observation and intensity variance data. The reference and computed transverse wave propagation speeds resulting from these characteristic frequencies are also shown ($2.45ms^{-1}$ and $2.21ms^{-1}$ respectively).

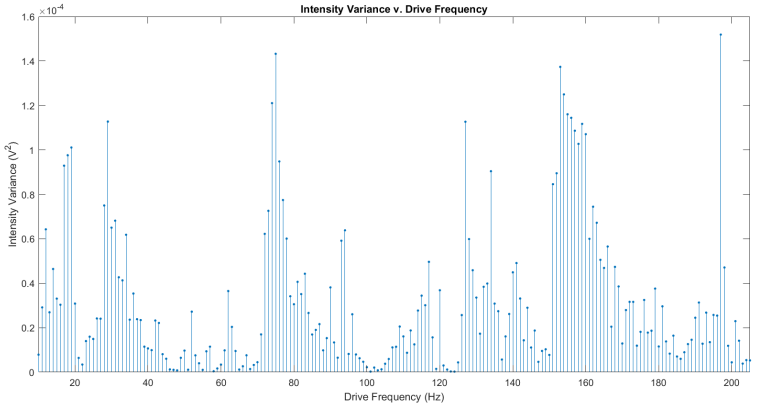

Figure 10: Temporal variance of the reflected light intensity for all drive frequencies in the range 10-205Hz. For normal modes, the the temporal variance is expected to be minimal.

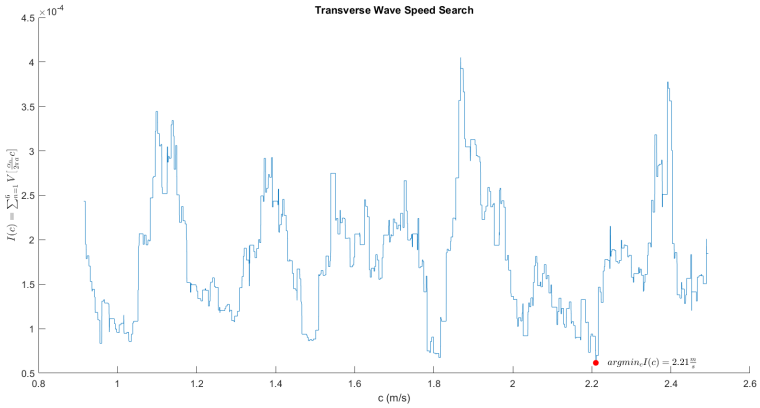

Figure 11: Objective function for finding transverse wave speed through soap bubble

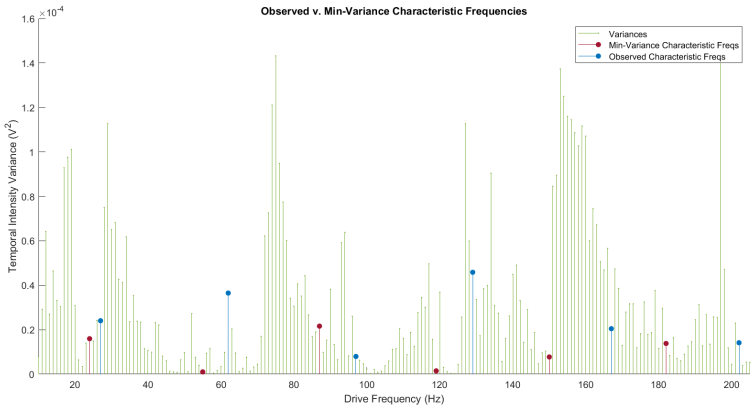

Figure 12: Comparison of the temporal intensity variances for characteristic frequencies f_1 through f_6 corresponding to the first six radially-symmetric modes identified via direct observation and our experimental approach.

4 Discussion

4.1 Experimental Results

We find the speed of transverse waves in a $7\,cm$ diameter soap bubble membrane to be $2.21\,ms^{-1}$ using the method proposed in this report. To assess the accuracy of our method, we compare our result to a reference speed calculated from the characteristic frequencies of the first six radially-symmetric modes visually observed in the frequency scan. Our reference speed is determined by averaging the solutions to Eqn. 1 for all observed characteristic frequencies, yielding $2.45\,ms^{-1}$. The difference between the computed speed and the reference speed constitutes a 10% error.

Another assessment of our method's fidelity compares the disparity between the observed and computed characteristic frequencies themselves. Examining Table 2 and Fig. 12, we see that the greatest disagreement is 20 Hz corresponding to f_6 while the minimum disagreement is 3 Hz corresponding to f_1. Generally, the discrepancy grows for higher values of n. Interestingly our method consistently undershoots the expected As it currently stands, the method presented herein offers a way of approximating the propagation speed of transverse waves in soap bubbles. In concluding, we suggest ways in which the method could be further refined.

4.2 Future Improvements

1. An additional validation step that was implied in the introduction involves measuring the constants in Eqn. 8 to determine an alternative reference speed independent of resonance-based techniques. While we did attempt to calculate this alternative reference speed to include in the report, we realized that we had incorrectly executed the procedure described in [4] to measure the constants. Consequently, the calculated reference speed was incompatible with our experimental results.

2. After collecting our data we realized that we neglected to account for the intrinsic frequency-dependent phase shift introduced to the acoustic drive signal by the second-order RC low-pass filter in our circuit. The frequency-dependent phase shift introduced by the filter is,

   $$\delta(f) = -2\arctan(2\pi f RC)$$

   This means that the strobe was not illuminating standing waves in the membrane at the peak of their oscillations as suggested in Fig. 5. This only slightly affects the constancy of the concatenated intensity measurements for standing waves. Still, the difference in temporal intensity variance between transient and standing waves would likely be more pronounced if the strobe offset properly accounted for the filter's effect.

3. The 1 Hz increment used for scanning through the acoustic drive frequency range is somewhat coarse. It is unlikely that the characteristic frequencies

of normal modes lie precisely at integer frequencies. Therefore, a potential improvement would simply be to decrease the size of the frequency increment, say perhaps to 0.1 Hz. This would ensure that the true characteristic frequencies of the membrane are more accurately identified.

4. Variations in the soap bubble surface density can be more rigorously characterized. Due to evaporation the concentration of surfactant in the bubble soap solution may vary over the course of the experimental period. Moreover, the bubble will inevitably pop over the course of experimental trials. Ensuring the surface density of the bubble remains consistent across these trials may produce more reliable data.

5 Supplementary Materials

- Data figures
- MATLAB scripts
- Hardware and system setup images

*** See attached figures and images ***

References

[1] Asmar, Nakhle H. *Partial Differential Equations with Fourier Series and Boundary Value Problems* 2nd ed. Chapter 4: Partial Differential Equations In Polar and Cylindrical Coordinates [pp. 193-268] (2000).

[2] Young, Peter. *UCSC Physics 116C Lecture Notes: The Orthogonality Relation Satisfied by Bessel Functions* (2009).
`http://physics.ucsc.edu/~peter/116C/bess_orthog.pdf`

[3] Morin, David. *Waves.* Chapter 7: 2D Waves and other topics. (Publication Pending)
`https://scholar.harvard.edu/david-morin/books`

[4] Sorensen, Carl D. *Measuring the Surface Tensions of Soap Bubbles* Brigham Young University
`https://ntrs.nasa.gov/archive/nasa/casi.ntrs.nasa.gov/19920021050.pdf`